Article

Experimental Study of Salicylic Acid as a Calcium Sulfate Dihydrate Scale Inhibitor, Analyzed from Surface Properties and Crystal Growth

Zhengwei Han,* Yu Xie, and Chenquan Ni

Read Online

| ACCESS | Metrics & More | Article Recommendations | SI Supporting Information |

ABSTRACT: Static and dynamic experiments were carried out to study the antiscale performance of salicylic acid (SA) to calcium sulfate dihydrate (CSD) scale. The CSD scale formed in the reuse of processing of wastewater of phosphorite flotation. The scale surface physicochemical properties have been investigated by means of scanning electron microscopy (SEM), transmission electron microscopy (TEM), X-ray diffraction (XRD), Fourier transform infrared spectroscopy (FTIR), ζ potential, and contact angle measurements. The antiscale mechanisms of SA to CSD were studied from surface properties and crystal growth. The results showed that the scale inhibition efficiency of SA to CSD reached 98.9% (6 mg/L) under static conditions. Under dynamic conditions, the faster the fluid velocity, the less CSD formed. The order of scaling capability on different material surfaces was 20#CS > 304SS > PC > PE. The growth of CSD was inhibited by SA resulting in the surface becoming porous. The deprotonated SA could easily interact with the Ca^{2+} to make the CSD surface potential negative. The wettability properties of the CSD are greatly improved when the contact angle is reduced. The surface tension values of CSD without and with 6 mg/L SA are 19.06 and 240.69 mN/m^2, respectively. SA as a scale inhibitor can significantly inhibit crystallization of CSD.
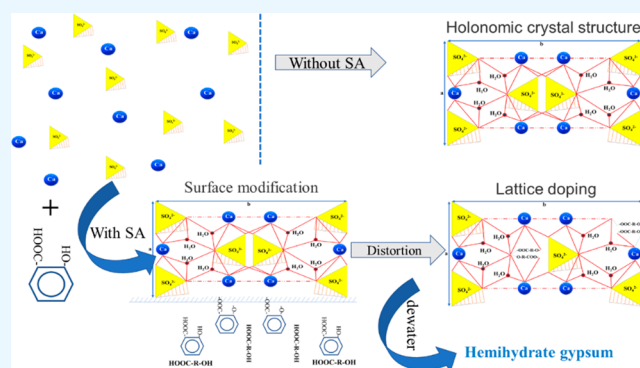
1. INTRODUCTION

The rapid development of phosphate rock beneficiation consequentially leads to increased water consumption and discharge. Wastewater reuse is an effective means to solve mine water scarcity and pollution. The wastewater of phosphorite flotation is usually acidic in a phosphorite mineral processing plant in Guizhou province. Sulfuric acid, the activator used in the flotation process, contributes a large number of hydrogen and sulfate ions to the wastewater. It also dissolves higher calcium, magnesium, phosphate, and other ions. As the number of reuse cycles of water increases, the scaling ions Mg^{2+}, Ca^{2+}, PO_4^{2-}, and SO_4^{2-} accumulate to a certain degree of supersaturation.[1] Lu et al. found that the main component of scale in the wastewater of phosphorite flotation is calcium sulfate dihydrate. With the increase of scale-forming ion supersaturation in wastewater, calcium sulfate dihydrate (CSD) scale on pipe surfaces is an inevitable phenomenon in the process of reusing wastewater.[2] The formation process of CSD scale can be simplified to calcium sulfate supersaturation solution developing into a crystal nucleus; then, the nuclei come together to formulate crystal precipitation and crystal growth into scale.[3] The cleaning of scale will increase the cost of industrial production. The prevention and control methods of scale formation mainly include the crystal seed method, scale inhibitor method, and chemical and physical cleaning method. Currently, an acceptable and widespread method is to use scale inhibitors for preventing scale formation.[4] This is attributed to scale inhibitors with high scale inhibition efficiency, low price, simple processing, and other properties. Mainstream researchers believe that the main mechanism of scale inhibition is the adsorption of functional groups to the growth site of scaling crystals. The crystal growth and nucleation rate are reduced due to the hydroxyl, carboxyl, amino, phosphoric acid, and other functional groups interacting with the scale surface.[5] Specifically, the functional groups hydrolyze to produce anions that are adsorbed to the active points on the crystal surface by electrostatic forces or double layer adsorption, which inhibits the growth of the crystal. Some researchers believe that the scale inhibition mechanism also includes solubilization, condensation, or dispersion. The specific mechanisms of solubilization, condensation, or dispersion are not clearly understood, but it is

believed that a common feature of threshold agents is sequestration or the capability of forming stable complexes with polyvalent cations.

In order to provide a reference for both fundamental study and applications, interaction mechanisms between scale and functional groups of scale inhibitors are an important research aspect.[6] Han et al.[7] have studied the scale in the wastewater of phosphorite flotation by static experiments. The performances of compound scale inhibitors were validated to inhibit crystal nucleation and growth. The effects of hardness, alkalinity, pH, and temperature on inhibition efficiency of the compound scale inhibitors were comparatively high. The scale inhibition mechanism has been the subject of a great number of studies. Dumazer et al.[8] have illustrated the effect of scale inhibitors on crystal growth dynamics and morphology of calcium sulfate by a classic nucleation theory model. Their results showed that scale inhibitors could effectively prolong the induction time of calcium sulfate crystallization and inhibit the longitudinal crystal growth. Azimi et al.[9] have carried out fundamental studies on the effect of surface energy on scale formation. Their results presented a fundamental understanding of scale formation as a function of surface energy attributes and provided insights for the design of scale-resistant surfaces with potential for technological applications.

Salicylic acid (SA) is a cheap and readily available extract from willow bark. The chemical name is *o*-hydroxybenzoic acid. Generally, at low concentrations, there have been no reports on the harm and toxicity of SA to human health and the environment. The functional groups of SA molecules include hydroxyl and carboxyl groups. It has a good complexing ability to calcium, magnesium, and iron ions. Meanwhile, its application as a scale inhibitor has not been well-reported. In this work, the performances of SA as a scale inhibitor for wastewater of phosphorite flotation have been investigated. The performances of SA for inhibition of CSD were assessed by static and dynamic experiments under different conditions. Scaling behaviors and scale inhibition corresponding mechanisms were further systematically investigated.

2. EXPERIMENTAL PROCEDURE

2.1. Materials. Calcium chloride, sodium sulfate, and SA were of analytically pure grade without further purification. Deionized water was purified once by a water purifier without further purification (18.2 MΩ/cm). A sodium ethylenediaminetetraacetic acid (EDTA) standard solution was prepared at a concentration of 0.01 mol/L.

2.2. Characterizations. High-purity water was prepared by a deionized water preparation machine (Exceed-E). The ζ potential and size distribution of CSD samples are characterized by ζ potential measurements and a laser particle size analyzer instrument (Delsa TM Nano). A multifunctional circulation temperature water bath was used to provide water baths of different temperatures from 20 to 60 °C. The samples were dried in a vacuum oven at 20 °C (DZF-6051). The contact angle of dihydrate calcium sulfate samples was measured by an optical contact angle meter (DSA-1000). N$_2$ adsorption−desorption curves of CSD and CSD treated with SA were obtained from automatic specific surface area measuring instrument. The surface areas were calculated with the Brunauer−Emmett−Teller (BET) method in the P/P_0 range 0.001−0.3, and the specific areas and pore structures were analyzed by the Barrett−Joyner−Halenda (BJH) method (Autosorb-1, Quanta chrome Instruments, America).[10] The phase composition, micro-

structure, and microstructure transformation of the minerals and materials were investigated by means of X-ray diffraction (XRD, Cu Kα radiation, λ = 0.154 06 nm), scanning electron microscopy and energy dispersive spectrometry (SEM-EDS, S-3400N, Hitachi), and high-angle annular dark field scanning transmission electron microscopy (TEM, Tecnai G2 F20, FEI Instrument). The XRD analysis was characterized by a X-Pert3 powder, Panalytical B.V., instrument with a scanning range of 2θ = 5−80° to gain information about the phase composition and crystallization of samples. Some physicochemical properties of the minerals and materials were also determined. The samples were pelletized using KBr at a mass ratio of 1/100 and then using Fourier transform infrared spectroscopy (FTIR) (Nicolet IS 50, Thermo) to confirm the functional groups. Determination of the valency of surface elements and their percentages was carried out with X-ray photoelectron spectroscopy (XPS; ESCALAB 250Xi, Thermo Fisher-VG Scientific), and all spectra were analyzed by XPS Peak 4.1 software after calibrating with a C 1s binding energy of 284.8 eV.[11]

2.3. Methods. *2.3.1. Static Scale Inhibition Experiments.* The static scale inhibition method is used to evaluate the scale inhibition ratio calculation. A certain concentration of supersaturation solution was prepared from calcium chloride and sodium sulfate. To be specific, a calcium chloride solution with a certain concentration of Ca^{2+} and a sodium sulfate solution with a certain concentration of SO$_4^{2-}$ were prepared, separately. The sodium sulfate solution and calcium chloride solution, of certain volumes, were quickly stirred to mix. The supersaturation solution was stored in a sealed condition in a 20 °C thermostat water bath for 24 h. The conditions of static scale inhibition experiments are shown in Table 1. CSD was prepared by simulative wastewater as shown in the following reaction equation:[12]

$$Na_2SO_4 + CaCl_2 + 2H_2O = CaSO_4 \cdot 2H_2O + 2NaCl$$
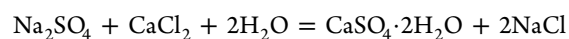
The Chinese national standard method (GB/T 16632-2008) was used to measure the concentration of Ca^{2+}. When the pH value of the solution was 12−13, calcium ions in aqueous solution were determined by EDTA standard solution with calcium carboxylic acid as a titration indicator. During titration,

Table 1. Conditions of Static Scale Inhibition Experiments

number	SA dosage (mg/L)	temperature (°C)	pH	supersaturation
1	2	20	6	3.09
2	4	20	6	3.09
3	6	20	6	3.09
4	8	20	6	3.09
5	10	20	6	3.09
6	12	20	6	3.09
7	14	20	6	3.09
8	6	30	6	3.09
9	6	40	6	3.09
10	6	50	6	3.09
11	6	60	6	3.09
12	6	20	2	3.09
13	6	20	3	3.09
14	6	20	4	3.09
15	6	20	5	3.09
16	6	20	7	3.09
17	6	20	6	1.55
18	6	20	6	6.17

EDTA formed a complex with free calcium ions. The end point of titration is when the solution color changes from purplish red to bright blue. The scale inhibition ratio calculation formula was as follows:[13]

$$\eta = \frac{C_a - C_b}{C_0 - C_b} \times 100\% \qquad (1)$$

The supersaturation ratio (S) was calculated as follows:[14]

$$S = \frac{c}{c^*} \qquad (2)$$

where η is the scale inhibition ratio, %; C_a is the equilibrium residual concentration of Ca^{2+} in the presence of the scale inhibitor, mg/L; C_b is the equilibrium residual concentration of Ca^{2+} without the scale inhibitor, mg/L; C_0 is the initial concentrations of Ca^{2+}, mg/L; S is the ratio of supersaturation; c is the CSD concentration, g/100 cm^3; and c^* is CSD (solute) solubility under the experimental conditions. The solubility of CSD is from 0.213 to 0.266 g/100 cm^3 when the solution temperature ranges from 20 to 60 °C.[15]

2.3.2. Dynamic Simulation Scale Inhibition Experiments. The dynamic simulation device was made by our laboratory as shown in Figure 1. The device consisted of a centrifugal pump,
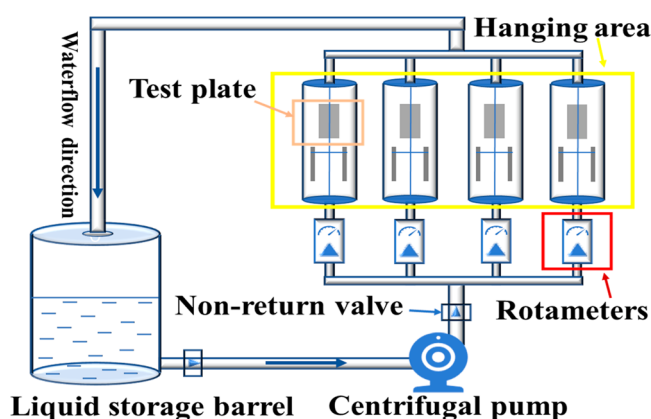

Figure 1. Schematic diagram of a dynamic scale inhibition test device.

four groups of rotameters, four groups of test plate hanging tubes, and a liquid storage barrel. The sample hanging test area of the round tube was composed of a transparent polycarbonate (PC) tube and a piece-hanging device, which can hang 8 pieces of sample. The liquid storage barrel was equipped with a temperature controller and heating device. Scaling and corrosion of the piece can be observed through the PC tube during the test. The equipment and parts used in the equipment were anticorrosive and high-pressure-resistant materials. The material of the test block is 20# carbon steel, PC, or PE (polyethylene of raised temperature resistance); all of their lengths, widths, and heights are 50, 25, and 2 mm, respectively. The conditions of dynamic simulation scale inhibition experiments are shown in Table 2. The calculation formula of surface scaling is shown as follows:

$$p = \frac{m - m_0}{s} \qquad (3)$$

where p is the amount of scaling per unit area, g/m^2; m_0 is the initial quality of the test block, g; m is the quality of the scale and test block, g; and s is the surface area of the test block, m^2.

Table 2. Conditions of Dynamic Scale Inhibition Experiments

number	dosage (mg/L)	temperature (°C)	flow speed (m/s)	plate material	supersaturation
1	0	25	1	PE	3.09
2	2	25	1	PE	3.09
3	6	25	1	PE	3.09
4	2	35	1	PE	3.09
5	2	45	1	PE	3.09
6	2	25	2	PE	3.09
7	2	25	4	PE	3.09
8	2	25	1	PC	3.09
9	2	25	1	20# carbon steel	3.09
10	2	25	1	304 stainless steel	3.09

3. RESULTS AND DISCUSSION

3.1. Experiments of Static Scale Inhibition. The effect of the dosage of SA (ortho-hydroxybenzoic acid, SA-OHBA) on scale inhibition was investigated for 24 h without stirring at concentration ranges from 2 to 14 mg/L. As shown in Figure 2A, under different dosages of SA, with the increase of SA dosage, the scale inhibition efficiency gradually increased, then remained stable, and finally decreased slightly. Specifically, when the dosage reached 6 mg/L, the scale inhibition efficiency remained unchanged and basically entered a stable stage. At this stage, the inhibition efficiency for CSD was 98.9% SA. Significantly, when the amount of scale inhibitors continues to increase, the scale inhibition efficiency gradually decreases because of the threshold effect of the scale inhibitor.[16]

One of the important factors affecting the scale inhibition efficiency of a scale inhibitor is temperature. The effect of temperature on scale inhibition was studied at the temperature range 293−333 K. The scale inhibition efficiency of SA as a function of temperature is shown in Figure 2B. The scale inhibition efficiency was found to decrease gradually as temperature increases. The solubility of CSD is variate at different solution temperatures. The reason for this behavior could be that higher temperature provides enough energy to the CSD molecules to overcome the activation energy of the dissolving reaction and speed up the transport of scale components from bulk solution to the crystal surface.[17]

The pH value of solution is an important factor to determine the hydrolysis and protonated reaction of heavy metal ions. As depicted in Figure 2C, when the pH value was in the range from 2 to 7, the scale inhibition efficiency of SA to CSD increased gradually with the increase in pH value. The solution pH was adjusted with hydrochloric acid and sodium hydroxide. According to Figure S1, the solubility of CSD did not change significantly from 0.2134 g/L to 0.2131 when the pH value was in the range from 2 to 7 at 25 °C. In lower-pH solutions, SA was more difficult to deprotonate because of the higher concentration of hydrogen ions. When the carboxylic acid group in the SA molecule was in a highly protonated state, it weakened the electrostatic adsorption with calcium sulfate. Therefore, the scale inhibition efficiency was worse in acidic conditions from the macroscopic point of view.[18]

Solution supersaturation is an important factor affecting the crystallization kinetics and behavior of scale deposits. In order to
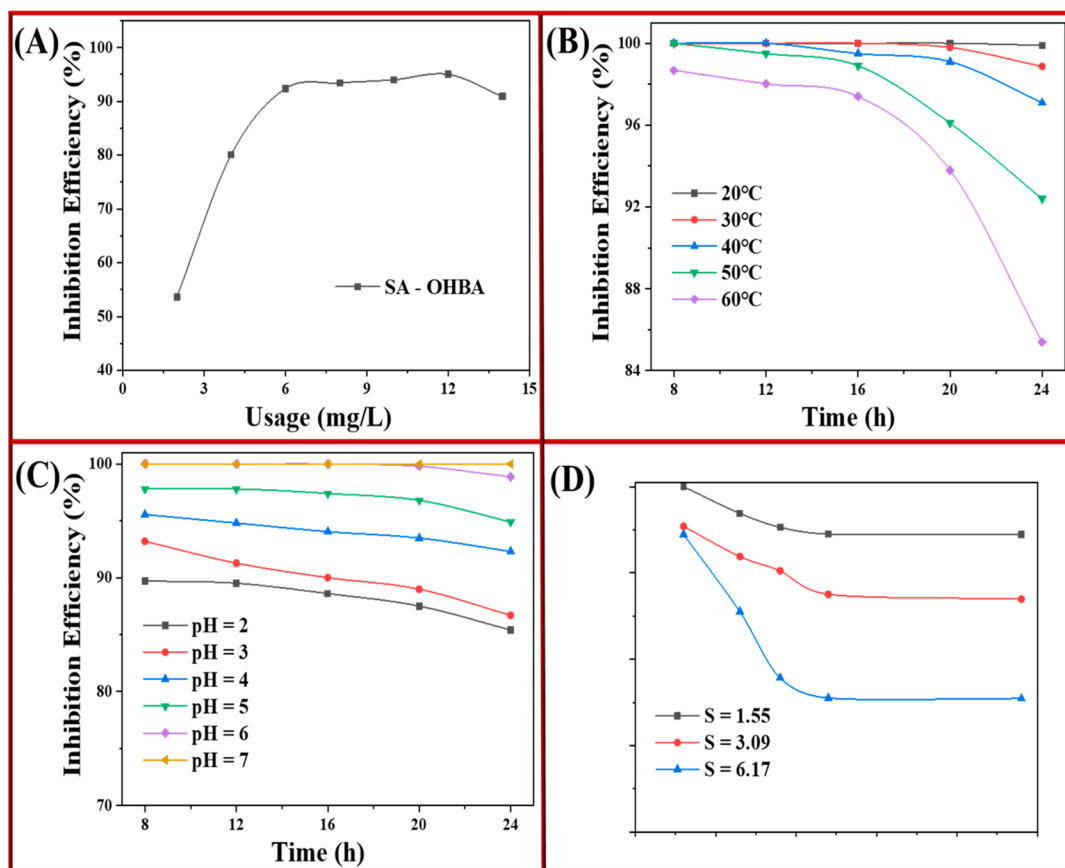
Figure 2. SA against CSD scale under different conditions: SA usage (A), temperature (B), pH value (C), and supersaturation (D).
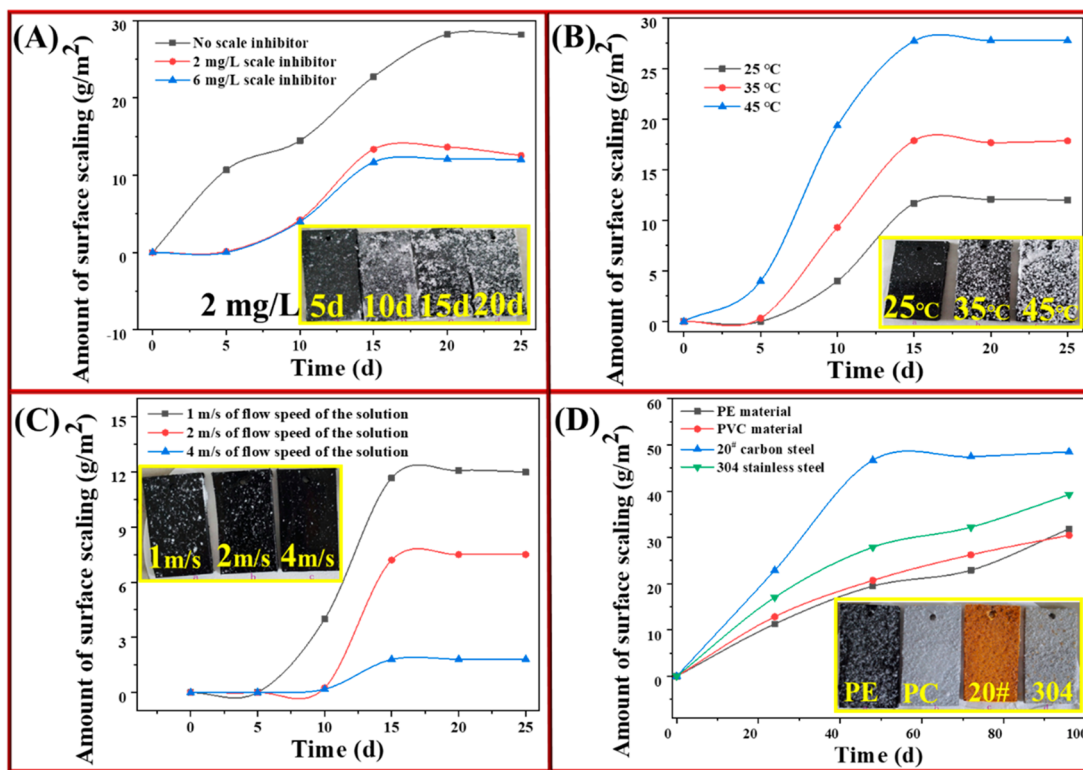

Figure 3. Effect of dynamic run time (A), fluid temperature (B), fluid velocity (C), and the material of the test plate (D) on amount of surface scaling.

investigate the effect of solution supersaturation on scale inhibition efficiency, the supersaturation experiments of ranges

from 1.55 to 6.17 were designed and carried out. As shown in Figure 2D, the higher the solution supersaturation was, the lower
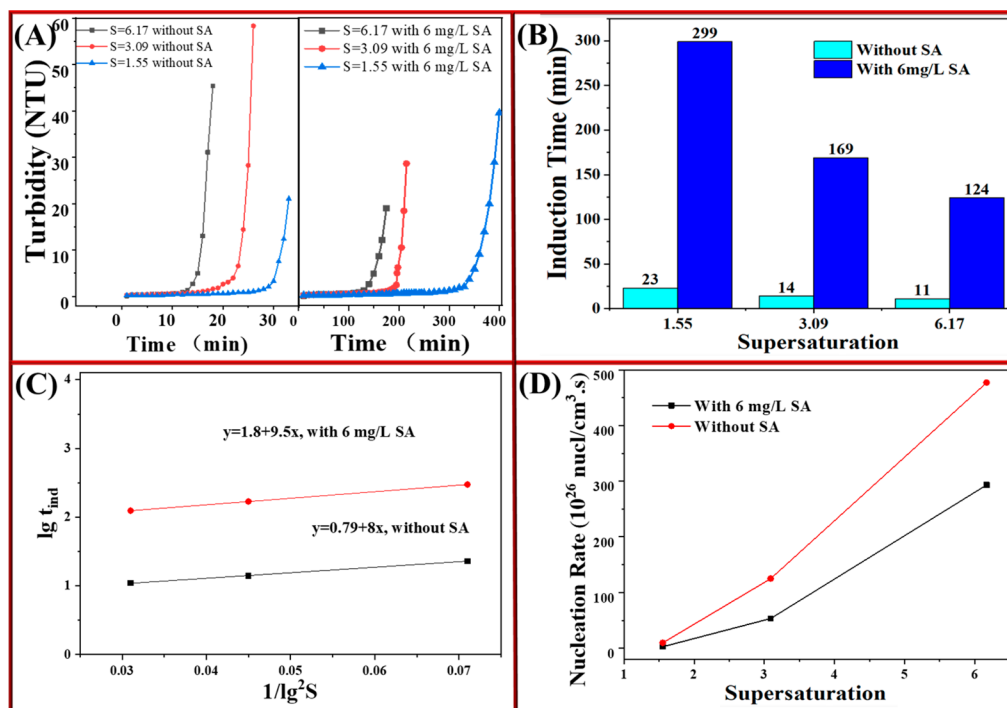
Figure 4. (A) Turbidity changes at different supersaturations. (B) Crystallization induction times varying at different supersaturations. (C) Fitting based on classical nucleation theory. (D) Nucleation rate changes at different supersaturations.

the scale inhibition efficiency was. When the time exceeded 12 h, the scale inhibition efficiency decreased slightly and entered the scale inhibition expiry stage. In general, with the increase of supersaturation, both nucleation rate and crystallization rate were increased.[19]

3.2. Experiments of Dynamic Scale Inhibition. In the actual process of reusing the wastewater from a phosphorite beneficiation plant, PC, PE, 20#CS, and 304SS materials are widely used. PC and PE pipes have been used in the long-distance delivery of wastewater. 20#CS and 304SS materials have mainly been used in pumps or mineral processing production equipment. Dynamic scale inhibition experiments are mainly to verify whether the amount of scale formation on the material surface can be reduced by scale inhibitors in the simulated fluid solution. As shown in Figure 3A, with the extension of dynamic time, the amount of scale on the plate surface increased gradually. After 20 days, the amount of scale tended to be stable in 28.1 g/m^2 without SA, 12.5 g/m^2 of 2 mg/L SA, and 10.4 g/m^2 of 6 mg/L SA. The amount of scale on the plate surface fluctuated at a certain value, which may be due to the balance between the adhesion force of scale and the shear force of the fluid. Obviously, compared with no addition of scale inhibitors, the amount of scale formation on the plate surface was significantly reduced by adding 2 and 6 mg/L scale inhibitor. In addition, with the increase of fluid temperature, the amount of scale on the plate surface increased obviously from 10.4 g/m^2 at 25 °C to 29.5 g/m^2 at 45 °C as shown in Figure 3B. In addition, Figure 3C reveals that the larger the fluid velocity was, the less scale there was on the plate surface. This may be due to the fact that as the flow velocity increased, the turbulent flow on the material surface increased, and the shear force of the fluid increased. This is because the shear force was greater than the adhesion force, and the scale cannot grow on the surface.[20] Furthermore, CSD had great different crystal growth habits on the surface of different materials. As shown in Figure 3D, the

amounts of scale on the PE, PC, 304 stainless steel, and 20# carbon steel plate surfaces were 10.8, 11.1, 17.4, and 23.8 g/m^2 on the thirtieth day; the order of scale formation capability on the surface was 20# > 304 > PC > PE. Therefore, in the actual scale inhibition process, PE material pipes and equipment should be selected first.

3.3. Analyses of Classical Nucleation Theory. Analyses of classical nucleation theory were associated with static test conditions. The purpose is to analyze the microscopic effect of scale inhibitor on the crystal nucleation process of scale, and to find the internal relationship between the microscopic effect and macroscopic phenomena. The homogeneous nucleation theory considers the particles to be spherical. The ions that make up the precipitate (also called crystal ions), which are associated by electrostatic action, spontaneously form the nucleus. Nucleation rate is defined as the number of formed nuclei per unit time per volume. It can be calculated according to the following relation:[21]

$$J = F \exp\left[\frac{-\beta\gamma^3 V_m{}^2 N_A f(\theta)}{(RT)^3 \ln^2 S}\right]$$

(4)

where J is the rate of nucleation, and F is a frequency constant, is known as the pre-exponential factor, and has a theoretical value of 10^{30} nuclei/(cm^3 s). β is a geometric (shape) factor of $16\pi/3$ for the spherical nucleus, and $f(\theta)$ is a correction factor. When purely homogeneous nucleation takes place, $f(\theta) = 1$, and when heterogeneous nucleation occurs, $f(\theta) = 0.01$. In this paper, purely homogeneous nucleation parameters are selected for discussion. V_m is the molar volume (74.69 cm^3/mol for CSD), T the absolute temperature (K), R the gas constant [8.314 J/(mol K)], γ the surface energy (J/m^2), and N_A Avogadro's number (mol^{-1}).

The change of surface potential reflects the change of surface energy. On the basis of the theory of classic homogeneous

nucleation, the induction time is related to the ratios of supersaturation as the following correlation:[22]

$$\lg(t_{ind}) = A + \frac{B}{T^3(\lg^2 S)} \tag{5}$$

$$J = Ce^{-\Delta G/KT} \tag{6}$$

where A, C, and K are empirical constants (dimensionless). B depends on the number of variables and is given by following correlation:

$$B = \frac{\beta\gamma^3 V_m^2 N_A f(\theta)}{(2.3RT)^3} \tag{7}$$

The relation between critical nucleus radius and free energy satisfies the following equation:

$$\Delta G = \frac{4}{3}\pi r^2 \gamma \tag{8}$$

where ΔG is the free energy of nucleation, representing the energy of crystal nucleus growth, J/m^2. r is the critical nucleation radius, cm. By fitting the relationship between supersaturation and induction time through eqs 5 and 7, nucleation rate and surface energy can be calculated. Through eq 6, the surface free energy of the crystal can be calculated. The critical radius of the crystal nucleus can be calculated by eq 8.

The variation trend of turbidity with time extension under different supersaturations is shown in Figure 4A. Except for the dosage of SA, the experimental details are listed in Table 1 (entries 3, 17, and 18). The time when the turbidity suddenly increases can be regarded as the induction time of crystallization.[23] The results of crystallization induction time are shown in Figure 4B. The addition of SA can effectively prolong the crystallization induction time of CSD. According to the analyses of our above experiments and results, the performance of SA closely relates to crystal nucleation rate. As shown in Figure 4C,D, The scale inhibitor can effectively reduce the nucleation rate of CSD. The nucleation rates (J) are 125×10^{26} and 53.37×10^{26} nuclei/(cm^3 s) without and with SA, respectively. The calculated surface energies (γ) are 1.38×10^{-6} and 1.46×10^{-6} J/m^2 without and with SA, respectively. By knowing the surface energy of CSD crystals (γ) and the nucleation rate (J), the crystallization free energy (ΔG) and critical nucleation radius (r) can be determined as listed in Table 3. It is clear that the crystallization free energy and critical

Table 3. Effect of SA on CSD Crystallization Free Energy and Critical Nucleation Radius

number	S	surface free energy ΔG (10^{-21} J/mol)		critical nucleation radius (10^{-8} cm)	
		without SA	6 mg/L SA	without SA	6 mg/L SA
1	1.55	33.79	40.3	7.6	8.1
2	3.09	21.3	25.5	6.1	6.5
3	6.17	14.82	17.19	5.1	5.3

nucleation radius were increased with 6 mg/L SA. The increase of crystallization free energy reduced the nucleation rate of CSD. Meanwhile, the larger critical nucleus radius also increased the resistance of crystal growth of CSD.

3.4. XRD Analysis. In order to investigate the crystal structure change of CSD before and after adding SA, XRD analysis results are shown in Figure 5A. The diffraction peak of

the sample without SA was mainly CSD, while the main diffraction peak of 11.63° was CSD, and the main diffraction peak of 14.658° was calcium sulfate hemihydrate (CSH). The relative contents of CSD and CSH in this sample are 95.1% and 4.9%, respectively, by semiquantitative analysis of the Scherer formula. After SA was added, the peak intensity of CSH at 14.658° increased obviously. The peak intensity of CSD at 11.63° decreased significantly. The relative content of CSH in the sample with 6 mg/L SA was about 18.8%. The internal reason for SA preventing the formation of CSD could be that SA, as a crystal modifier, converted part of CSD into CSH.[24]

3.5. FTIR Analysis. Figure 5B shows the FTIR spectra of CSD and CSD treated by antiscalant. The peaks located at 3554 and 3409 cm^{-1} were attributed to O−H stretching vibrations of the crystallized water of CSD. Peaks at 3244 cm^{-1} were ascribed to the bending bands of the free water. The peaks at approximately 1686 and 1621 cm^{-1} were attributed to O−H bending vibrations of the crystallized water of CSD.[25] The peaks at approximately 1143 and 1114 cm^{-1} were attributed to γ_3 stretching vibrations of the SO$_4^{2-}$. The peaks at approximately 669 and 600 cm^{-1} were attributed to γ_4 stretching vibrations of the SO$_4^{2-}$.[26] Compared with the spectrum of CSD, the spectrum of CSD treated by SA contained three new peaks. The peaks located at 1446 and 893 cm^{-1} were attributed to the bending vibration of C−H bonds (−CH$_2$, −CH$_3$) and aromatic hydrocarbons, respectively. In addition, in the spectrum of CSD treated by SA, a C−H bending vibration peak of monosubstituted benzene was observed at approximately 761 cm^{-1}. These results indicated that SA was successfully adsorbed onto the surface of CSD, while in other regions of the spectrum, there are characteristic peaks of CSD. There is no Ca−O vibration peak or C−Ca vibration peak found in the FTIR spectrum. The main reason for this phenomenon could be that there was no chemical interaction between SA and Ca^{2+}.[27]

3.6. Morphology Analysis. The SEM photographs of dihydrate calcium sulfate without and with 6 mg/L SA are shown in Figure 6A,E. A significant difference can be observed between the surface topographies of dihydrate calcium sulfate in that the external surface of dihydrate calcium sulfate with SA has a rough texture with a large number of cavities, and the crystal of dihydrate calcium sulfate without any scale inhibitors was needle-shaped.[28] The TEM photographs of dihydrate calcium sulfate without scale inhibitors are shown in Figure 6B−D. Those revealed an ordered lattice arrangement of naturally crystallized CSD. In addition, the TEM photographs of dihydrate calcium sulfate with 6 mg/L SA are shown in Figure 6F−H. The lattice arrangement was disordered, and the spacing between 033 and 020 could be measured. The growth of calcium sulfate crystals can be viewed as in strict accordance with a certain crystal lattice forming a dense and hard crystal. The scale inhibitor was adsorbed on the crystal and doped in the lattice.[29] The surface becomes loose and porous. The crystal is easy to break into a granular or short flat shape and hinders the growth of calcium sulfate scale.[30]

3.7. Specific Surface Areas and Grading Analysis. The surface of CSD treated by SA became loose and porous after the crystal distortion, which will inevitably lead to the change of the distribution of particle apertures. Nitrogen (N$_2$) adsorption−desorption isotherms and pore size distributions of CSD and CSD treated by SA are shown in Figure 7A,B. The results showed that the BET specific surface area of CSD is 2.41 m^2/g, whereas the specific surface area of CSD treated by SA increased to 14.73 m^2/g. In addition, the average pore diameter of CSD
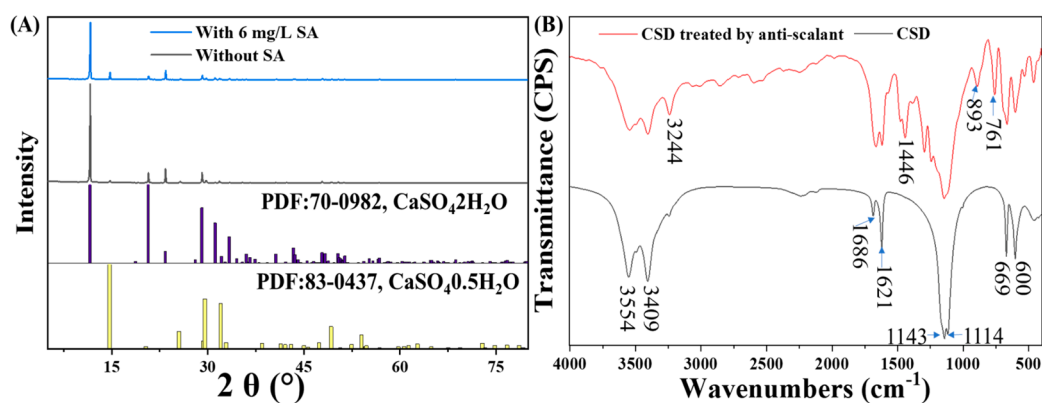
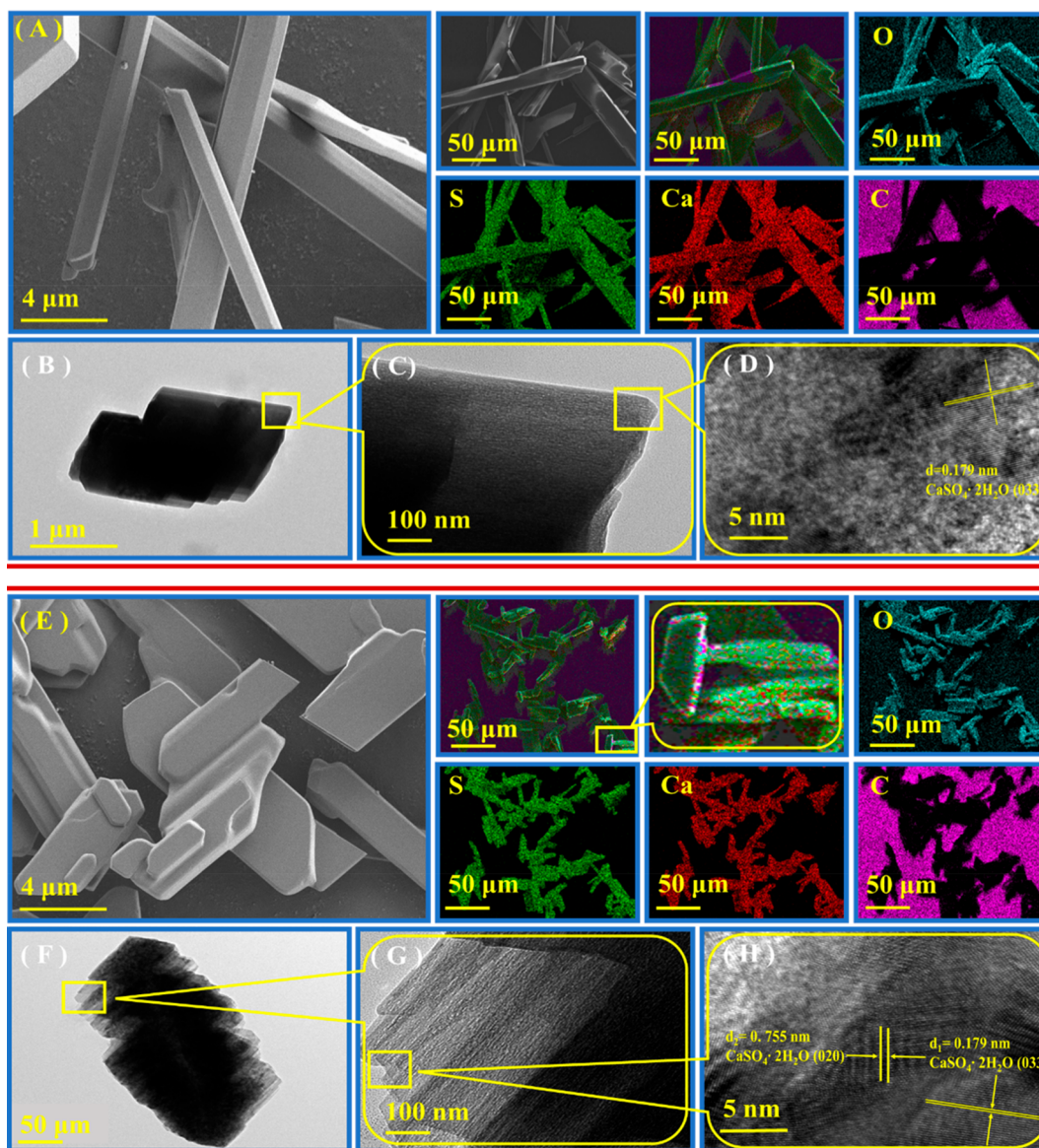**Figure 5.** Results of XRD analysis (A) and FTIR analysis (B).

Figure 6. SEM photographs of dihydrate calcium sulfate without SA (A) and with 6 mg/SA (E). TEM photographs of dihydrate calcium sulfate without SA (B−D) and with 6 mg/SA (F−H).

treated by SA (17.65 nm) is larger than that of CSD (2.54 nm). This can be explained by the fact that as SA was adsorbed onto the CSD surface, the CSD particles became larger and porous.[31]

Meanwhile, the inhibition of crystal growth may result in the change of grain size distribution. The particle size distributions of CSD and CSD treated by SA are shown in Figure 7C,D. The
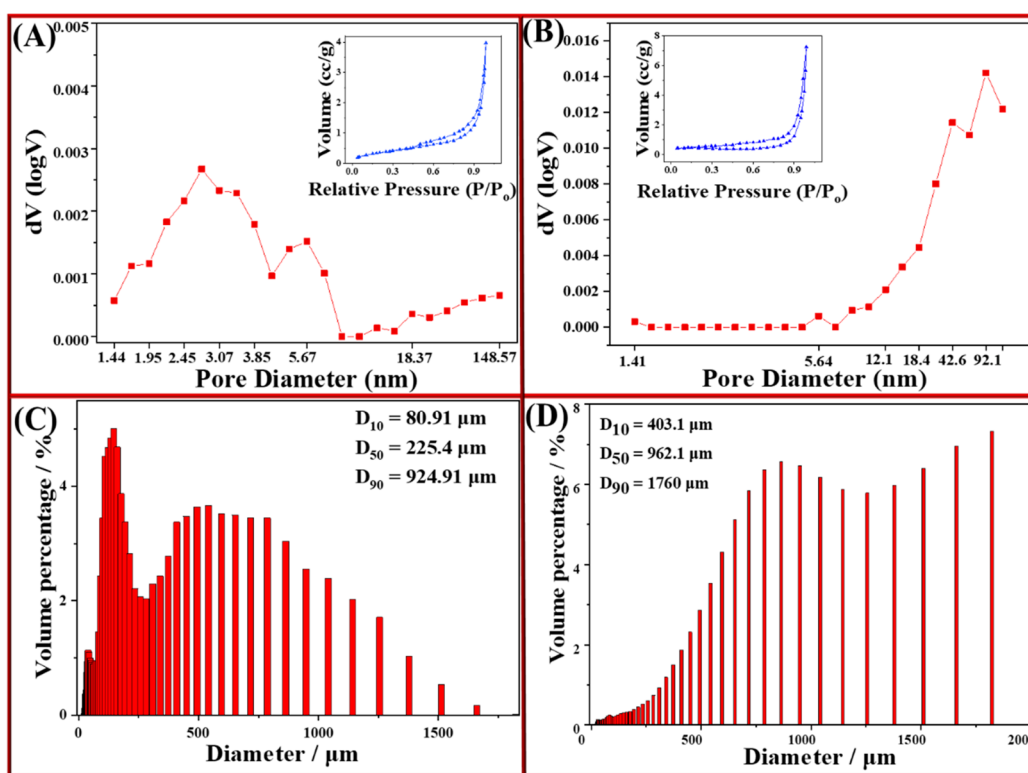
Figure 7. N$_2$ adsorption−desorption isotherms and pore size distributions of CSD (A) and CSD treated by SA (B). Statistical results of the particle size distribution of CSD (C) and CSD treated by SA (D).

statistical results of the particle size distribution of CSD without scale inhibitors are $D_{10} = 80.91$ μm, $D_{50} = 225.4$ μm, and $D_{90} = 924.91$ μm. The statistical results of the particle size distribution of CSD treated by 6 mg/L SA are $D_{10} = 403.1$ μm, $D_{50} = 962.1$ μm, and $D_{90} = 1760$ μm. The average particle size of CSD treated by SA is significantly larger than that of CSD. Scale inhibitors can effectively inhibit the longitudinal growth and promote the transverse growth of gypsum crystals.

3.8. Surface Potential and Contact Angle Analysis. The scale inhibition phenomenon of the scale inhibitor attracted to the Ca^{2+} active site or the surface of CSD crystallite would influence the contact angle of the sample. As shown in the Figure 8A,B, the contact angle of the CSD surface is 115.8°; the contact angle of CSD treated by SA is 7.1°. The scale inhibitor group and

the blank space group contrast shows a notable difference. Scale generated from supersaturation solution with 6 mg/L SA tended to be hydrophilic. The result shows that the wettability properties of the scale are greatly improved when the contact angle reduces. Wettability is an important property of surfactants.[32] SA as a surfactant can increase the interfacial tension of CSD and effect crystal growth, so it will be used extensively. The crystal surface of CSD treated with SA was hydrophilic. During the crystal secondary growth process, additional energy was required to overcome the hydration film on the surface when crystal grains were connected to each other.

To investigate the surface energy, we analyzed contact angles of the above samples derived based on the Young equation and Fowkes theory of liquid−liquid interfacial tension as follows:[33]

$$\cos\theta = \frac{\gamma_{SG} - \gamma_{SL}}{\gamma_{LG}} \tag{9}$$

$$\gamma_{SL} = \gamma_{LG} + \gamma_S - 2(\gamma_S^d \gamma_{LG}^d)^{1/2} \tag{10}$$

$$\gamma_S = \gamma_S^d + \gamma_S^p \tag{11}$$

where θ is the contact angle, deg; γ_{SG} the surface tension between solid and gas, mN/m^2; γ_{SL} the surface tension between solid and liquid, mN/m^2; γ_{LG} the surface tension between liquid and gas, mN/m^2; γ_S the surface tension of solid, mN/m^2; γ_S^d the dispersion component of surface tension of solid, mN/m^2; γ_S^p the polarity component of surface tension of solid, mN/m^2; and γ_{LG}^d the dispersion component of surface tension between liquid and gas, mN/m^2.

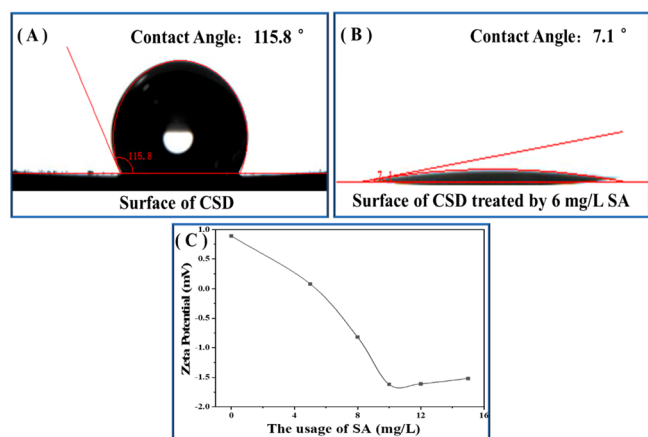Equation 12 can be derived from eqs 9−11 as follows:

Figure 8. (A) Contact angle of CSD. (B) Contact angle of CSD treated by SA. (C) Surface ζ potential change.

$$\cos\theta = -1 + \frac{2(\gamma_S^d \gamma_{LG}^d)^{1/2}}{\gamma_{LG}} \tag{12}$$

We regard γ_S as approximate to γ_S^d and already knew that $\gamma_{LG} = 72.8$ mN/m^2, and $\gamma_{LG}^d = 21.8$ mN/m^2. We calculated the surface tension of each group using eq 12. Calculated surface tension (γ_S) is reported in Table 4.

Table 4. Effect of SA on CSD Surface Tension

experiments	contact angle θ (deg)	$\cos\theta$	γ_S (mN/m^2)
empty group	115.8	−0.44	19.06
test group	7.1	0.99	240.69

According to Table 4, the surface tension of CSD before and after being treated by SA is 19.06 and 240.69 mN/m^2, respectively. SA as a scale inhibitor can significantly increase the surface tension of CSD. The change regularity of surface tension is consistent with the changing rule of crystallinity and crystallite size, all supporting the previous research conclusions.[6]

The adsorption of SA on the CSD surface will inevitably lead to a change in surface potential. Hydrolysis of the scale inhibitor produces amine groups, phosphonic acid groups, and carboxylic acid groups, each with negative charge. During a collision between the scale inhibitor and the Ca^{2+} active site or the CSD crystallite, physical or chemical scale inhibition phenomena occurred in the surface of the CSD crystallite. Then, it lead to the formation of an electrical double layer with negative charge on the surface of the microcrystal. As shown in Figure 8C, the ζ potential of the CSD surface declined from 0.83 to −1.79 mV with the dosage increasing. As the scale inhibitor continued to increase, the CSD surface potential stabilized at −1.8 mV. Most likely, there was a greater amount of deprotonation groups with increasing dosage. Deprotonation of SA can interact with the metal ions, such as Ca^{2+}, to form an electrical double layer. The value of the ζ potential of the CSD crystallite reaches the minimum when the dosage of the scale inhibitor is 6 mg/L. When we continue to add compound into the solution, the value increases. This means that the scale inhibition ability on the Ca^{2+} active site or the surface of the CSD crystallite is weakened. The degree of hydrolysis reached saturation. In addition, with the content of carboxyl groups and amine groups in solution increased, it is easy to have an interaction with the other divalent ion in the water, resulting in the function of bridging. It is easy to produce gel precipitation, resulting in the decrease of the relative content of inhibitors.[9]

3.9. XPS Analysis. To further investigate the laws for the microstructure development of CSD before and after treatment by SA, XPS was used to characterize the elemental oxidation status. Figure 9 presents the XPS spectra of CSD and CSD treated by SA. Table 5 shows the content and binding energy of surface elements. Compared with CSD, the surface element valence states of CSD treated by SA did not change. It is obvious that the relative content of Ca element reduced from 17.24% to 14.91%; the relative content of S element reduced from 20.12% to 18.5%, and the relative content of C element increased significantly from 11.87% to 18.3%. If the reason for the increase of the relative content of C element was CO$_2$ gas adsorbed on the surface of CSD, then the relative content of O element must also increase. In fact, the opposite is true. The relative content of O element decreased from 50.77% to 48.56%. Those results indicated that the increase of C element was caused by the adsorption of SA on the CSD surface. In addition, compared
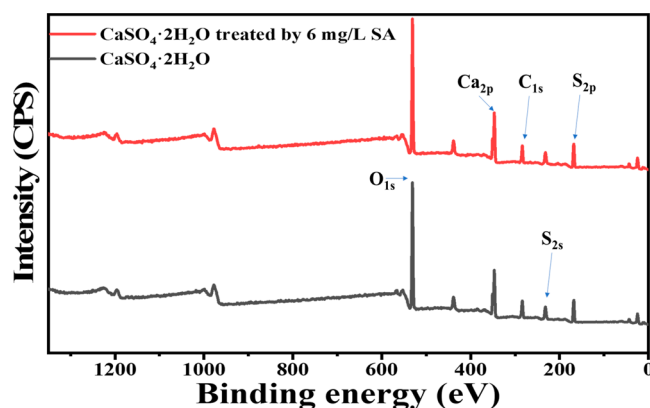

Figure 9. XPS spectra of CSD and CSD treated by 6 mg/L SA.

Table 5. Analysis of Surface Elements on CSD and CSD Treated by SA with XPS

sample	elements	binding energy (eV)	content (%)
CSD	Ca 2p	348.68	17.24
	O 1s	531.85	50.77
	C 1s	285.06	11.87
	S 2p	169.16	20.12
CSD treated by SA	Ca 2p	348.68	14.91
	O 1s	531.85	48.56
	C 1s	285.06	18.3
	S 2p	169.16	18.5

with the CSD, the binding energies of Ca 2p, C 1s, and S 2p on the surface of CSD treated by SA have slightly decreased or increased. Thus, SA would be grafted onto the CSD surface by physical adsorption.[34]

3.10. Scale Inhibition Mechanism Analysis. According to the above analysis and characterization, there is a possible mechanism for preventing calcium sulfate scaling of SA described in Figure 10. First, the scale inhibition mechanism of SA was based on classical crystallization theory. As a scale inhibitor, SA was added into the supersaturated solution of calcium sulfate, which interfered with the homogeneous nucleation of calcium sulfate crystals at the initial growth stage. As a result, in the process of the formation of calcium sulfate crystal, part of the lattices were doped by scale inhibitor molecules. Thus, both the microstructure and the lattice matrix were negatively affected. On the other hand, scale inhibitor molecules adhered to and modified the surface of CSD by electrostatic adsorption, which prevented CSD from growing along the longitudinal direction. Therefore, the macroscopic morphology, surface potential, contact angle, and particle size distribution have undergone significant changes. Moreover, as a crystal modifier, SA dehydrated CSD into CSH. Compared with calcium sulfate dihydrate, hemihydrate calcium sulfate is more soluble. Therefore, dehydration of CSD into CSH may be one of the important mechanisms for SA to exert its scale inhibition effect.

4. CONCLUSION

In our work, SA as a scale inhibitor showed an excellent scale inhibition ability under static and dynamic conditions. Under static conditions, the scale inhibition efficiency of SA to CSD was above 90% when temperature, acidity, and supersaturation were changed. The optimal scale inhibition efficiency is 98.9% of 6 mg/L SA. The scale inhibition efficiency was found to decrease
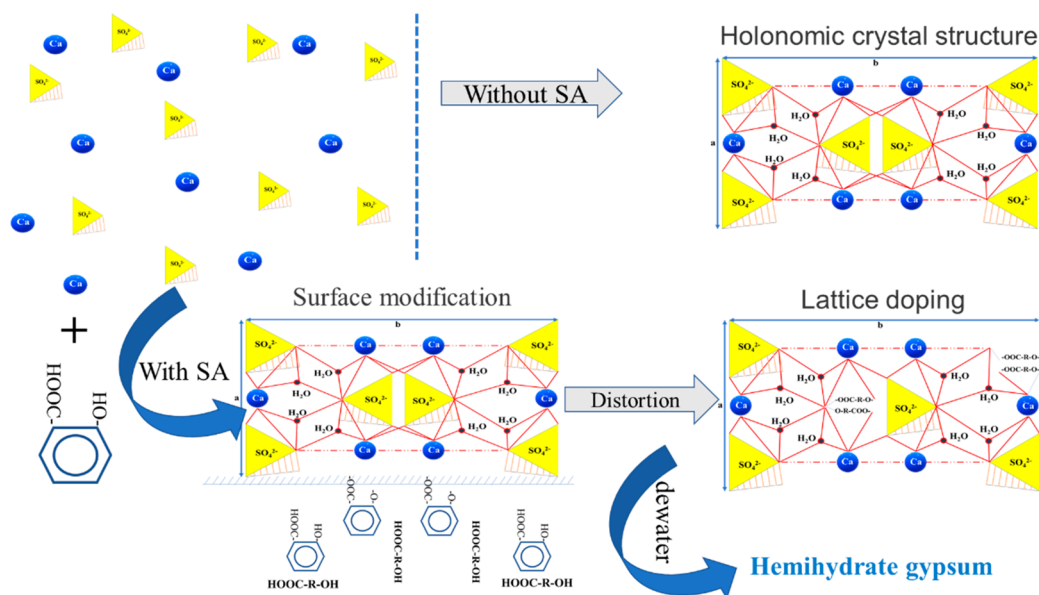
Figure 10. Mechanisms of SA preventing CSD scaling.

gradually as temperature increased. The induction time increased more than 11-fold in the presence of 6 mg/L SA at the supersaturation ratio of 3.09. When the carboxylic acid group in the SA molecule was in a highly protonated state, it weakened the electrostatic adsorption with CSD. Under dynamic conditions, SA can effectively reduce the scaling amount of CSD on the surface of different materials by changing the flow rate, temperature, and supersaturation. The mechanisms of SA preventing CSD scaling included lattice doping, surface modification, and dewatering.

ASSOCIATED CONTENT

Supporting Information

The Supporting Information is available free of charge at https://pubs.acs.org/doi/10.1021/acsomega.2c01262.

Relationship between pH and solubility of CSD (PDF)

AUTHOR INFORMATION

Corresponding Author

Zhengwei Han − *School of Minerals Processing and Bioengineering, Central South University, Changsha 410083, China;* orcid.org/0000-0003-2845-2845; Email: 1040055211@qq.com

Authors

Yu Xie − *School of Minerals Processing and Bioengineering, Central South University, Changsha 410083, China*

Chenquan Ni − *School of Minerals Processing and Bioengineering, Central South University, Changsha 410083, China*

Complete contact information is available at:
https://pubs.acs.org/10.1021/acsomega.2c01262

Author Contributions

We confirm that the manuscript has been read and approved by all named authors and that there are no other persons who satisfied the criteria for authorship but are not listed. We further confirm that the order of authors listed in the manuscript has been approved by all of us.

Notes

The authors declare no competing financial interest.

REFERENCES

(1) Lu, C.; Liu, Z.; Meng, Y.; Han, Z.; Zhao, H. Research on effect of parameters for quality of backwater in phosphate flotation on pipeline scaling. *Indust. Miner. & Proce.* **2017**, *46*, 4−7.

(2) Zhang, S.; Qu, H.; Yang, Y.; Fu, C.; Tian, Z.; Yang, W. Scale inhibition performance and mechanism of sulfamic/amino acids modified polyaspartic acid against calcium sulfate. *Desalination.* **2017**, *419*, 152−159.

(3) Gryta, M. The influence of magnetic water treatment on CaCO$_3$ scale formation in membrane distillation process. *Sep. Purif. Technol.* **2011**, *80*, 293−299.

(4) Abdel-Aal, E. A.; Abdel-Ghafar, H. M.; Anadouli, B. E. New Findings about Nucleation and Crystal Growth of Reverse Osmosis Desalination Scales with and without Inhibitor. *Cryst. Growth. Des.* **2015**, *15*, 5133−5137.

(5) Davey, R. J.; Schroeder, S. L. M.; Horst, J. H. Nucleation of Organic CrystalsA Molecular Perspective. *Angew. Chem., Int. Ed.* **2013**, *52*, 2166−2179.

(6) Liu, Y.; Zou, C.; Li, C.; Lin, L.; Chen, W. Evaluation of β-cyclodextrin−polyethylene glycol as green scale inhibitors for produced-water in shale gas well. *Desalination.* **2016**, *377*, 28−33.

(7) Han, Z.; Liu, Z.; Zhang, Q.; Meng, Y. Anti-scaling study on phosphate rock flotation wastewater. *Desalin. Water Treat.* **2018**, *101*, 53−60.

(8) Dumazer, G.; Narayan, V.; Smith, A.; Lemarchand, A. Modeling Gypsum Crystallization on a Submicrometric Scale. *J. Phys. Chem. C* **2009**, *113*, 1189−1195.

(9) Azimi, G.; Cui, Y.; Sabanska, A.; Varanasi, K. K. Scale-resistant surfaces: Fundamental studies of the effect of surface energy on reducing scale formation. *Appl. Surf. Sci.* **2014**, *313*, 591−599.

(10) Zeng, Q.; Li, S.; Sun, W.; Hu, L.; Zhong, H.; He, Z. Eco-friendly leaching of rubidium from biotite-containing minerals with oxalic acid and effective removal of Hg^{2+} from aqueous solution using the leaching residues. *J. Clean. Prod.* **2021**, *306*, 127167.

(11) Zeng, Q.; Li, S.; Sun, W.; Hu, L.; Zhong, H.; He, Z. High adsorption capacity and super selectivity for Pb(II) by a novel adsorbent: Nano humboldtine/almandine composite prepared from natural almandine. *Chemosphere.* **2020**, *253*, 126650.

(12) Oshchepkov, M.; Golovesov, V.; Ryabova, A.; Redchuk, A.; Tkachenko, S.; Pervov, A.; Popov, K. Gypsum Crystallization during Reverse Osmosis Desalination of Water with High Sulfate Content in

Presence of a Novel Fluorescent-Tagged Polyacrylate. *Crystals.* **2020**, *10*, 309−319.

(13) Mady, M. F.; Ortega, R.; Kelland, M. A. Exploring Modified Alendronic Acid as a New Inhibitor for Calcium-Based Oilfield Scales. *Energy Fuel.* **2022**, *36*, 1863−1873.

(14) Maher, Y. A.; Ali, M. E. A.; Salama, H. E.; Sabaa, M. W. Preparation, characterization and evaluation of chitosan biguanidine hydrochloride as a novel antiscalant during membrane desalination process. *Arab. J. Chem.* **2020**, *13* (30), 2964−2981.

(15) Abdel-Aal, E. A.; Abdel-Ghafar, H. M.; El-Sayed, D.; El-Shazly, A. N.; Hoinkis, J. Crystallization study of reverse osmosis desalination scales at low salinity with and without inhibitor. *Particul. Sci. Technol.* **2017**, *35*, 749−754.

(16) Al-Roomi, Y. M.; Hussain, K. F. Application and evaluation of novel acrylic based CaSO4 inhibitors for pipes. *Desalination.* **2015**, *355*, 33−44.

(17) Rahman, F. Calcium sulfate precipitation studies with scale inhibitors for reverse osmosis desalination. *Desalination.* **2013**, *319*, 79−84.

(18) Khormali, A.; Petrakov, D. G.; Moghaddam, R. N. Study of adsorption/desorption properties of a new scale inhibitor package to prevent calcium carbonate formation during water injection in oil reservoirs. *J. Petrol. Sci. Eng.* **2017**, *153*, 257−267.

(19) Mady, M. F.; Rehman, A.; Kelland, M. A. Synthesis and Antiscaling Evaluation of Novel Hydroxybisphosphonates for Oilfield Applications. *ACS Omega.* **2021**, *6*, 6488−6497.

(20) Yi-Tsung Lu, A.; Kan, A. T.; Tomson, M. B. Nucleation and Crystallization Kinetics of Barium Sulfate in the Hydrodynamic Boundary Layer: An Explanation of Mineral Deposition. *Cryst. Growth Des.* **2021**, *21*, 1443−1450.

(21) Chandra-ambhorn, S.; Tungtrongpairoj, J.; Jutilarptavorn, A.; Nilsonthi, T.; Somphakdee, T. On the hot-rolled recycled carbon steels: their oxide formation, pickling ability and scale adhesion. *Anti-Corros. Method. M.* **2019**, *66*, 294−299.

(22) Younes, A. A.; El-Maghrabi, H. H.; Ali, H. R. Novel polyacrylamide-based solid scale inhibitor. *J. Hazard. Mater.* **2017**, *334*, 1−9.

(23) Fu, H.; Guan, B.; Jiang, G.; Yates, M. Z.; Wu, Z. Effect of Supersaturation on Competitive Nucleation of CaSO$_4$ Phases in a Concentrated CaCl$_2$ Solution. *Cryst. Growth Des.* **2012**, *12*, 1388−1394.

(24) Hu, H.; Hale, T.; Yang, X.; Wilson, L. J. A spectrophotometer-based method for crystallization induction time period measurement. *J. Cryst. Growth.* **2001**, *232*, 86−92.

(25) Zhang, X.; Ran, L.; Wang, X.; Jin, B.; Zhang, J.; Li, S.; Yang, L. Structural characteristic and formation mechanism of hemihydrate calcium sulfate whiskers prepared using FGD gypsum. *Particuology.* **2022**, *62*, 98−103.

(26) Altaş, L.; Balkaya, N.; Cesur, H. Pb(II) Removal from Aqueous Solution and Industrial Wastewater by Raw and Lime-Conditioned Phosphogypsum. *Int. J. Environ. Res.* **2017**, *11*, 111−123.

(27) Lee, C.; Don, T.; Lin, D.; Chen, C.; Cheng, L. Characterization of acrylic copolymers applied in negative-type photoresist via a ternary composition diagram. *J. Appl. Polym. Sci.* **2008**, *109*, 467−474.

(28) Li, J.; Chen, S.; Sheng, G.; Hu, J.; Tan, X.; Wang, X. Effect of surfactants on Pb(II) adsorption from aqueous solutions using oxidized multiwall carbon nanotubes. *Chem. Eng. J.* **2011**, *166*, 551−558.

(29) Rahman, F. Calcium sulfate precipitation studies with scale inhibitors for reverse osmosis desalination. *Desalination.* **2013**, *319*, 79−84.

(30) Al-Roomi, Y. M.; Hussain, K. F. Application and evaluation of novel acrylic based CaSO$_4$ inhibitors for pipes. *Desalination.* **2015**, *355*, 33−44.

(31) Chen, Y.; Zhou, Y.; Yao, Q.; Bu, Y.; Wang, H.; Wu, W.; Sun, W. Preparation of a low-phosphorous terpolymer as a scale, corrosion inhibitor, and dispersant for ferric oxide. *J. Appl. Polym. Sci.* **2015**, *132* (6), 41447.

(32) Li, M.; Hu, L.; Zhong, H.; He, Z.; Sun, W.; Xiong, D. Efficient removal of diethyl dithiocarbamate with EDTA functionalized electrolytic manganese residue and mechanism exploration. *J. Hazard. Mater.* **2021**, *410*, 124582.

(33) Tröger, J.; Lunkwitz, K.; Bürger, W. Determination of the Surface Tension of Microporous Membranes Using Contact Angle Measurements. *J. Collo. Interface Sci.* **1997**, *194*, 281−286.

(34) Duan, Z.; Li, J.; Li, T.; Zheng, S.; Han, W.; Geng, Q.; Guo, H. Influence of crystal modifier on the preparation of α-hemihydrate gypsum from phosphogypsum. *Constr. Build. Mater.* **2017**, *133*, 323−329.